PCCP

Constant Chemical Potential Cycles for Capacitive Deionization

Journal:	*Physical Chemistry Chemical Physics*
Manuscript ID	CP-ART-09-2019-005032.R1
Article Type:	Paper
Date Submitted by the Author:	17-Oct-2019
Complete List of Authors:	Moreno, Daniel; University of Kentucky, Center for Applied Energy Research Hatzell, Marta; Georgia Institute of Technology, George W. Woodruff School of Mechanical Engineering

PCCP

ARTICLE TYPE

Cite this: DOI: 00.0000/xxxxxxxxxx

Constant Chemical Potential Cycles for Capacitive Deionization †

Daniel Moreno[a] and Marta C. Hatzell*[a]

Received Date
Accepted Date

DOI: 00.0000/xxxxxxxxxx

The primary energy consuming operations which occur within a Capacitive Deionization (CDI) cell, are the ion removal (electrosorption), ion concentrating (electrodesorption), and solution switching processes. In theory the maximum system performance for a CDI system arises when solution switching occurs while maintaining a fixed number of ions (N), and when electrosorption/desorption occurs while maintaining a fixed chemical potential (μ). These fixed state variable based operations are analogous to the Carnot cycle, where heat transfer occurs at constant temperature and compression and expansion occur while maintaining constant entropy. In reality, maintaining a constant number of ions during switching is not practically feasible, thus here we investigate two alternative cycles where switching instead occurs while maintaining constant charge or voltage. Unlike constant number of ions, maintaining charge and voltage constant is feasible using a potentiostat. These theoretical cycles were chosen as they are analogues or ideal-like (Stirling and Ericsson) cycles, which are also practically feasible. The thermodynamic analysis reveals that these alternative cycles provide an avenue to approach the theoretical limit with low saline feed water; however, they are not capable of approximating ideal operations at elevated feed-water concentrations.

1 Introduction

The efficiency of any capacitive deionization (CDI) cycle is dependent on the system operating conditions (voltage limit, temperature, feed salinity) and chosen thermodynamic process path [1–8], Ultimately, minimizing energy consumption and maximizing thermodynamic efficiency is achieved when the conditions and process paths are optimized. Slight changes in either can result in significant energy savings, as over the lifetime of a CDI device, a cycle is repeated thousands of times [6,8]. There are numerous thermodynamic process paths which can be utilized to get a desired degree of desalination. A well studied example of this is when electroadsorption/desorption occurs while maintaining a constant current or constant voltage. Both approaches can achieve the same desired ion removal, while experimental evidence suggests that constant current-based desalination may be more energy efficient [9–13]. These differences are largely tied to the thermodynamic trajectory of the ion removal process.

While constant current and constant voltage ion removal processes are the most employed processes used to electrochemically remove ions, there are theoretically a number of other state variables which could be held constant to achieve the same degree of desalination. The thermodynamically ideal operating mode is defined by drawing an analogy between the CDI cycle and a Carnot (ideal) cycle [14]. Thus, optimum operation incorporates electroadsorption/desorption processes which maintain a constant chemical potential, and switching processes which maintain a constant number of ions. In reality, maintaining a constant number of ions, like maintaining constant entropy, is not technically feasible. Therefore, there is a need to define alternative practical trajectories which can effectively mimic those found within the Carnot analogy cycle.

Here, we aim to compare the performance of two ideal-like thermodynamic cycles with the ideal Carnot-analog cycle. The two alternative cycles are chosen based on analogies drawn between thermal processes and electrochemical processes using differential relations for free energy and work [14]. The chosen ideal-like cycles resemble the Stirling and Ericsson cycles, which are well known to be technically practical and exhibit performance which approachs the Carnot limits. In each cycle, the adsorption/desorption occurs while maintaining a constant chemical potential condition, while the switching step differs in each cycle. Cycle operation is demonstrated on a chemical potential versus number of ions diagram and a charge versus voltage diagram. Finally, the impact of feed salinity (C_0) and salt removal ($\Delta C/C_0$) is explored in each cycle.

[a] 771 Ferst Drive NW, 316 J. Erskine Love Bldg , Atlanta, GA USA. Tel: 01 404 385 4503 E-mail: marta.hatzell@me.gatech.edu

† Electronic Supplementary Information (ESI) available. See DOI: 10.1039/cXCP00000x/

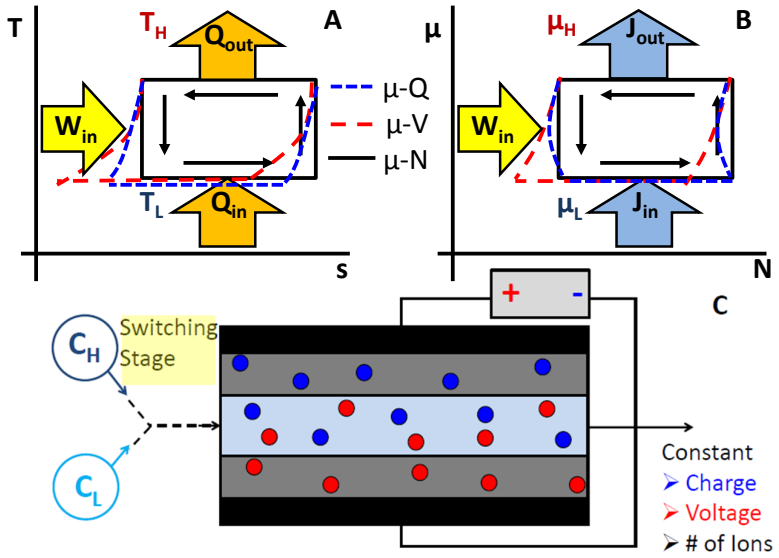

Fig. 1 (A) Thermodynamic cycle, (B) deionization cycle, and (C) depiction of a CDI solution switching process. During this process, we investigate the cycle energetics associated with maintaining constant charge, voltage, and constant number of ions.

2 Methodology

The cycles examined in this study are based on the Gouy Chapman Stern (GCS) theory for the electrochemical double layer of the capacitor. The cycles operate under infinitely slow conditions, eliminating the need for transient-based considerations such as the diffusion and resistance of the cell.

When one stream during the desalination process is diluted, the other is subsequently concentrated into a brine stream. The magnitude of the concentration in this brine stream C_B is determined by the influent and dilute concentrations C_0 and C_D, and the water recovery ratio α:

$$C_B = \frac{C_0 - \alpha C_D}{1 - \alpha} \tag{1}$$

where α is the recovery ratio, or fraction of the water that is sent to the dilute stream. Cycles that employ constant concentration stages consequently have only two defined concentrations: the dilute concentration C_D, and the brine concentration C_B defined in Eq. 1. The rationale is that in fully reversible, infinitely slow cycles, the initial concentration will only be seen at the influent for a very short time before charging/discharging. The cycles are run under infinitely slow conditions by linearly scaling a chosen parameter during each process until the desired final value is met at the next state. This eliminates irreversibilities due to transients in thermodynamic processes. As the cycles are run under the assumption of infinitely slow conditions, challenges associated with adsorption capabilities of electrodes are also neglected in this study. Recent experimental work into flowable electrodes[4,15] provides one practical example into how such high adsorption capabilities for CDI may be practically attainable. Lastly, while material considerations are not taken into account for the CDI cell or electrodes, constant values such as the Stern layer capacity are borrowed from previous experimental observations and computational studies.

Each of the cycles tested operates in four stages: In the first process, the cell concentration switches from the brine concentration to the dilute concentration. For the second process, the cell undergoes charging under a constant chemical potential (concentration) until a maximum cell voltage of 1.2 V is reached. In the third process, concentration is switched once again to the brine concentration values. For the fourth and last process, the cell is discharged until the starting voltage of 0.1 V is reached, returning the cycle to its starting conditions.

In CDI cycles, switching stages involve returning the dilute stream to the initial inlet concentration[16,17]. Here, due to the constant chemical potential operation of the CDI cycles, the concentrations are immediately switched to the dilute stream concentration (before charging) or to the brine stream concentration (before discharging). When transients are no longer considered, the switching mode happens much more rapidly than the charging or discharging stages, and during each of those stages the cell concentration reaches equilibrium with either the dilute or brine streams[5]. The discharge voltage was constrained at 0.1 V primarily to allow for energy recovery during the discharging stage. Additionally, this discharge value of 0.1 V was chosen based on previous studies and subsequently built upon here[5,18].

For all of the cycles tested, the charging and discharging processes take place at a constant chemical potential. The chemical potential μ varies as a function of both concentration and temperature:

$$\mu = k_B T ln\left(\frac{C}{C_{ref}}\right) \tag{2}$$

where k_B is Boltzmann's constant and C_{ref} is a reference temperature to the environment, taken here as 1 M[19]. If the cycle is run under isothermal conditions, constant chemical potential

Table 1 Thermodynamic state proprieties for thermal and electrochemical processes.

Cycle	Thermal Properties	Electrochemical Properties
Ericsson	T,P	μ, V_{cell}
Stirling	T,V	μ, σ
Carnot	T,S	μ, N

is achieved by ensuring that cell concentration is held constant during either a charging or discharging phase. In a constant CDI experiment run in continuous mode, a constant current operation can maintain a desired concentration depending on the current applied and system parameters[5,20,21]. As all cycles evaluated here are isothermal, constant chemical potential processes are equivalent to constant concentration processes.

During switching stages, the property kept constant depends on the type of cycle operated (Table 1). The cycle operations correspond to analogies for thermodynamics for both heat engines and refrigerators: Stirling (μ-Q) cycles employ constant surface charge, Ericsson (μ-V) cycles employ constant cell voltage, and Carnot (μ-N) cycles use a constant number of ions (Figure 1C). The number of ions term is unique in that it considers both the concentration in the cell and its surface charge:

$$N = \Gamma + CL_eN_{av} \tag{3}$$

where N_{av} is Avogadro's constant, L_e represents the pore length between carbon electrode particles (pore volume/pore area, taken as 4 nm in this study), and Γ is the excess surface charge. We use the pore length L_e as an arbitrary characteristic length to relate between volume-based and area-based terms.

Γ is determined as a function of both the electrode surface charge σ and additional crossover charge σ^*

$$\Gamma = (\sigma + \sigma^*)^2 - \sigma^* \tag{4}$$

$$\sigma^* = \frac{1}{(2\pi\lambda_B\lambda_D)} \tag{5}$$

where the Debye and Bjerrum lengths for the electrolyte, λ_B and λ_D, determine the crossover charge[17,19]. All simulations run in this study assume a double layer Bjerrum length of 0.7 nm. The crossover charge is defined as the charge at which attractive forces from counter ions and repulsive forces from co-ions are balanced[22].

All tests conducted in this study are run at standard room conditions, so constant chemical potential stages can also be interpreted as constant concentration stages. For reversible processes, a stage with a constant number of ions is analogous to an adiabatic process.

The GCS model for the EDL divides the total cell voltage into two components: voltage in the rigid Stern layer, which varies proportionally as a function of charge, and the diffuse layer, which varies with both charge in the cell and the length of the layer (Debye length) itself. The diffuse layer voltage ΔV_D is given as

$$\Delta V_D = 2V_T sinh^{-1}\Big(\frac{\sigma\sqrt{(\pi\lambda_B)}}{2CN_{av}}\Big) \tag{6}$$

with thermal voltage V_T defined as V_T = RT/F, where F is Faraday's constant. For the Stern layer voltage ΔV_{st}, Gauss' law is used for a 1:1 electrolyte (as in the case with NaCl):

$$\Delta V_{st} = \frac{\sigma e}{C_{st}} \tag{7}$$

where C_{st} is the Stern capacity and e is the elementary charge. Previous studies using GCS models have assumed a constant Stern capacity around 0.2 F/m^2 [23,24]. To further assess the validity of cycling performance with regards to different pore lengths, we also examine additional cycles employing the modified Donnan (mD) model which accounts for micropore concentrations. We employ a version of the mD model which takes into account attractive forces within micropores[25], and is applicable to a wide range of concentrations such as the one employed in this study.

Assuming a symmetric cell configuration, the diffuse and Stern layer potentials can be combined and doubled for both sides of the cell to provide the total cell voltage ΔV_{cell}:

$$V_{cell} = 2(\Delta V_{st} + \Delta V_D) \tag{8}$$

Integrating cell charge over the total voltage of the cycle gives the total work input needed to drive the cycle. In addition to comparing this work for different cycle operations, this cycle work is also related to the minimum cycle work required to drive the cycle (based on concentrations and recovery ratios). Another goal with the cycle operation is to reduce the net energy consumed as close as possible to the minimum (Gibbs) energy of mixing ΔG_{mix}:

$$\Delta G_{mix} = nRT\Big[\frac{C_0}{\alpha}ln\Big(\frac{C_0 - \alpha C_D}{C_0(1-\alpha)}\Big) - C_D ln\Big(\frac{C_0 - \alpha C_D}{C_D(1-\alpha)}\Big)\Big] \tag{9}$$

This cycle thermodynamic efficiency denoted as η_{TEE}, is given by:

$$\eta_{TEE} = \frac{\Delta G_{mix}}{E_{net}} \tag{10}$$

where E_{net} is the total amount of energy expended within the cycle, that is, the amount of energy expended during charging after subtracting the amount recovered during discharging. For brackish water concentrations, values for η_{TEE} typically do not exceed 10%[1,26]. Changes in the TEE for different cycles will be evaluated by looking at the concentration change (C_0 - C_D) relative to the initial concentration. This ratio displays performance parameters relative to a given removal percentage.

3 Results and Discussion

By employing Equations 2-8 under the operating modes presented, CDI cycles can be depicted using either charge-voltage (Q-V) diagrams or chemical potential-number of ions (μ-N) diagrams, by plotting each of the individual points as the form a cycle. For each of the cycles depicted, the area enclosed in the μ-N diagram equals the total work consumed during one charge-discharge cycle. With a C_0 = 20 mM, α = 0.5 and C_D = 1 mM, the

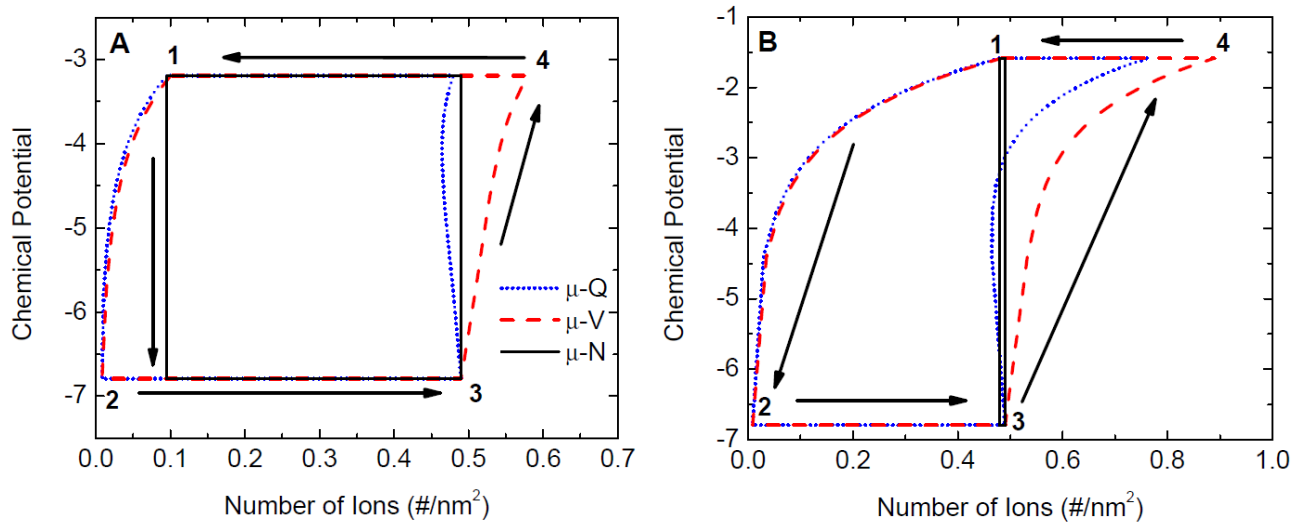

Fig. 2 Constant potential-number of ions diagrams for (A) C_0=20 mM and (B) C_0=100 mM.

energy consumed was 2.0 kWh/m^3 (0.14 Joules/Coulomb)) for the μ-V cycle, 1.8 kWh/m^3 (0.17 J/C) for the μ-Q cycle, and 1.6 kWh/m^3 (0.15 J/C) for the μ-N cycle (Figure 2A). Thus by altering the state variable during the switching stage (process 1-2 and process 3-4) the entire cycle energy consumption is altered. However, the energy consumption difference from cycle to cycle only differed by approximately 20%. This is visible through the differences in cycle area as demonstrated on the μ-N diagram (Figure 2A). However, when the the feed water concentration increases, the deviation between the areas increases substantially (Figure 2B). With elevated feedwater concentration (C_0=100 mM), the difference between the curves differ by as much as 400%.

The difference in the energy consumption can be discerned through inspecting the various thermodynamic trajectories for the four processes used within the desalination cycle (solution switching, adsorption, solution switching and desorption).

During the initial switching stage (process 1-2), the cell's voltage increases for each case, however, the magnitude differs. This increase in voltage is due to the changes in the structure of the electric double layer with concentration. At lower concentrations, the Debye length expands, leading to a voltage jump (Figure SI1). When the initial feed was 20 mM, switching while maintaining a fixed number of ions (iso-N), resulted in the greatest voltage rise (400 mV). Conversely, the voltage rise experienced during switching with iso-V was 0 mV, and iso-Q was 50 mV. To minimize the energy consumed during charging, it is ideal for the voltage rise during switching to be maximized, as this reduces the charge needed to reach a desired set voltage (V_{max}). In the case of the constant number of ions, the voltage rise corresponds with an increase in charge, which also reduces the required input energy.

During process 2-3 the cell is charged, while the feed stream is desalinated. Since the feed and minimum concentration are fixed, the ions removed are the same for each cycle. However,increasing

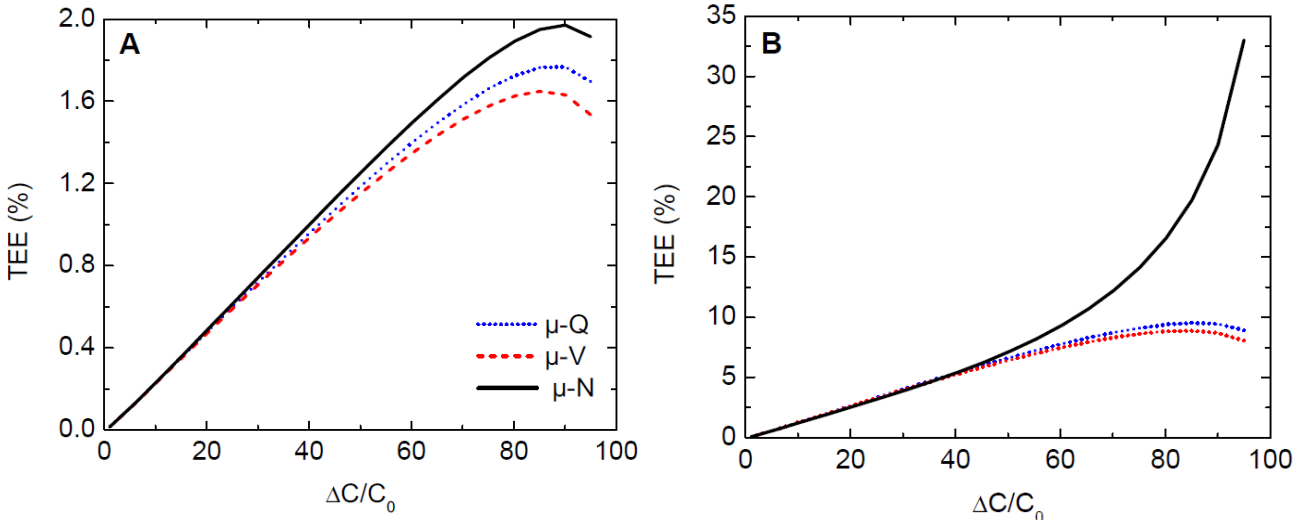

Fig. 3 Thermodynamic energy efficiency as a function of percentage of salt removed for (A) C_0=20 mM and (B) C_0=100 mM.

the cell voltage during the switching stage (process 1-2), reduced the energy that is required to achieve the desired ion removal. With a 20 mM feed, the energy input for process 2-3 was 7.9 kWh/m^3 (0.72 J/C) for the μ-V cycle, 7.9 kWh/m^3 for the μ-Q cycle (0.72 J/C) and 7.3 kWh/m^3 (0.82 J/C) for the μ-N cycle. Thus, the lower energy input for the μ-N cycle is a direct result of the switching process operations.

During process 3-4, the feed is switched with the brine solution prior to discharge. During this stage, the surface charge must decrease for the iso-N cycles, in order to maintain a fixed N at the higher brine concentration. As a result, the maximum cycle charge is nearly 5% less than in the case of the μ-V cycles. This is non-ideal as decreasing the charge and voltage prior to discharging results in lower energy recovery. While most CDI systems do not recover energy during the discharge process, it is necessary in order to achieve high thermodynamic efficiency.

Finally, during process 4-1, the feed is discharged and returned to the initial concentration and voltage. During this stage, the discharge allows for an additional amount of energy recovered. All processes perform this discharge at the same constant chemical potential, but begin at different charge and cell voltage values based on the previous switch stage employed. The μ-Q cycle recovers 6.0 kWh/m^3 (0.55 J/C) and the μ-V cycle recovers 8.6 kWh/m^3 (0.67 J/C). Finally, the μ-N cycle recover nearly the same energy.

While the above demonstrates the importance of feed concentration, the degree of salt removal also impacts the thermodynamic efficiency. For the case of feed water at 20 mM, all three cycles exhibit a consistent linear increase in the TEE with increased salt removal (Figure 3A). However, a maximum is reached at approximately 95% desalination, after which the work input increases exponentially at a rate faster than ΔG_{mix} increases (Figure SI2A). For the constant number of ions cycle (μ-N), this maximum is subsequently increased to 2% compared to 1.6% for the constant voltage switching (μ-V), and 1.8% for the constant charge switching (μ-Q). Therefore, with low salinity feed streams, and low salt removal ($\Delta C/C_0 <$50%), the three cycles are nearly identical. This is consistent with thermal energy systems, where Ericsson and Stirling cycles tend to approach the Carnot limit in some operating conditions. If employing the mD model, the maximum efficiencies near 95% removal are still observed for all three modes of operation (Figure SI 3A), although the values are lower due to the greater charge buildup in the overlapping double layers of the mD model. While the mD model does not yield the highest efficiencies for the μ-N operation, although performance does exceed the μ-V cycle with more dilute streams, suggesting that the μ-N cycle works best at higher concentration ranges.

When the concentration is 100 mM, the μ-Q and μ-V cycles follow a similar trend, with the maximum TEE approaching 10% at 95% removal. However, the μ-N cycle increases substantially without experiencing a tradeoff at high salt removal. Furthermore, the peak theoretical TEE approaches $>$ 30% which is in line with membrane based systems. Thus, the difference between the energy consumed for each cycle, only differs at high concentrations and with high salt removals. Even at high concentrations, the various ideal-like cycles are able to produce similar performance up until ($\Delta C/C_0 =$50%). This is confirmed even for the mD model: While efficiencies are overall lower, when the μ-V and μ-Q modes cycles approach maximum TEE values of 5% and 6%, the μ-N cycle reaches a peak TEE of nearly 8% (Figure SI3B). As the mD model employed here takes into account attractive ionic forces at higher concentrations, it is more applicable in both high and low concentration ranges. By evaluating both EDL models and observing the same trend with improved TEE here, the benefits of the Carnot analogs can be further expanded upon.

When evaluating the cycle work consumed as a function of desalination degree, a maximum in the cycle work for the mu-N cycle is observed, at a desalination degree of approximately 40%. This means that at lower concentrations, less work is consumed due to the narrower μ range, but at higher concentrations, less work is consumed due to the narrower range imposed by the constant number of ions condition. The corresponding trend in cycle work can est be visualized when viewed on a μ-N diagram (Figure 4A), with much smaller changes in the number of ions at higher concentrations. The maximum in the net cycle work for the μ-N mode of operation is more clearly seen when sweeping over the full range of inlet concentrations between 20 and 100 mM (Figure 4B). Net work consumption for the μ-Q and μ-V modes of operation are also plotted for reference. The maximum value for the μ-N operational mode can also provide a suggestion for the target ranges at which a μ-N cycle can be employed, for desalination in practical cycles is challenging at higher concentration ranges. Even at the maximum net work of $C_0 \approx$ 50 mM consumes almost 10% less work than its next closest competitor, the μ-Q cycle.

4 Conclusion

Three thermodynamic cycles which contain constant chemical potential charging and discharging stages were investigated. The cycles differed based on the thermodynamic process employed during solution switching. Through investigating the impact of solution switching while maintaining iso-N, iso-V and iso-Q processes, we were able to compare the performance of the thermodynamic analog Carnot, Ericsson and Stirling cycles. The Carnot cycle is not practically executable in an electrochemical system, and therefore detailing the differences between these cycles may provide insight into feasible ways to achieve ideal-like performance. The results suggest that the use of iso-V and iso-Q solution switching processes can enable near ideal performance if the cell is operated with low feed water concentration ($C_0<$20 mM), or low salt removal ($\Delta C/C_0 <$50%). However, the difference between the ideal and ideal-like cycle can differ by as much as 400% as the feed water concentration is increased or the total salt remove approaches 100%.

Conflicts of interest

The authors declare that there is no conflict of interest.

Acknowledgments

This material is based upon work supported by the National Science Foundation under Grant No. 1821843.

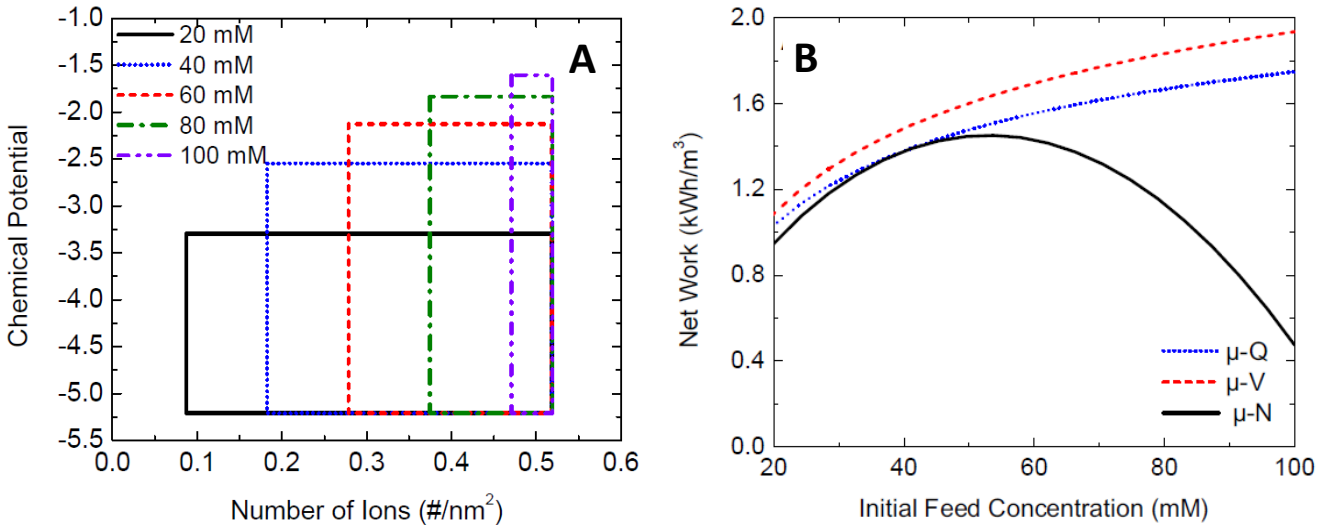

Fig. 4 (A) Chemical potential-number of ions diagram for a Carnot analog (μ-N) cycle with a constant 5 mM dilute stream and various inlet concentration streams. (B) Cycle work consumed for constant chemical potential charging cycles with a 5 mM dilute stream and various input feed concentrations.

References

1 R. Zhao, S. Porada, P. Biesheuvel and A. Van der Wal, *Desalination*, 2013, **330**, 35–41.

2 J. Dykstra, R. Zhao, P. Biesheuvel and A. Van der Wal, *Water research*, 2016, **88**, 358–370.

3 X. Shang, R. D. Cusick and K. C. Smith, *Journal of The Electrochemical Society*, 2017, **164**, E536–E547.

4 D. Moreno and M. C. Hatzell, *Industrial & Engineering Chemistry Research*, 2018, **57**, 8802–8809.

5 D. Moreno and M. C. Hatzell, *ACS Sustainable Chemistry & Engineering*, 2019, 11334–11340.

6 A. Ramachandran, D. I. Oyarzun, S. A. Hawks, M. Stadermann and J. G. Santiago, *Water research*, 2019, **155**, 76–85.

7 M. Qin, A. Deshmukh, R. Epsztein, S. K. Patel, O. M. Owoseni, W. S. Walker and M. Elimelech, *Desalination*, 2019, **455**, 100–114.

8 S. A. Hawks, J. M. Knipe, P. G. Campbell, C. K. Loeb, M. A. Hubert, J. G. Santiago and M. Stadermann, *Water research*, 2018, **129**, 327–336.

9 J. Kang, T. Kim, K. Jo and J. Yoon, *Desalination*, 2014, **352**, 52–57.

10 Y. Qu, P. G. Campbell, L. Gu, J. M. Knipe, E. Dzenitis, J. G. Santiago and M. Stadermann, *Desalination*, 2016, **400**, 18–24.

11 D. Moreno, Y. Bootwala, W.-Y. Tsai, Q. Gao, F. Shen, N. Balke, K. B. Hatzell and M. C. Hatzell, *Environmental Science & Technology Letters*, 2018, **5**, 745–749.

12 R. Zhao, P. Biesheuvel and A. Van der Wal, *Energy & Environmental Science*, 2012, **5**, 9520–9527.

13 J. Dykstra, S. Porada, A. van der Wal and P. Biesheuvel, *Water research*, 2018, **143**, 367–375.

14 R. van Roij, *Electrostatics of Soft and Disordered Matter*, 2014, **263**, year.

15 S.-i. Jeon, H.-r. Park, J.-g. Yeo, S. Yang, C. H. Cho, M. H. Han and D. K. Kim, *Energy & Environmental Science*, 2013, **6**, 1471–1475.

16 L. Wang, P. Biesheuvel and S. Lin, *Journal of colloid and interface science*, 2018, **512**, 522–528.

17 P. M. Biesheuvel, *J. Colloid Interface Sci.*, 2009, **332**, 258–264.

18 D. Moreno and M. C. Hatzell, *The Journal of Physical Chemistry C*, 2018, **122**, 22480–22486.

19 N. Boon and R. Van Roij, *Molecular Physics*, 2011, **109**, 1229–1241.

20 L. Wang and S. Lin, *Environmental science & technology*, 2018, **52**, 4051–4060.

21 J. Zhang, K. B. Hatzell and M. C. Hatzell, *Environmental Science & Technology Letters*, 2017, **4**, 470–474.

22 T. Markovich, D. Andelman and R. Podgornik, *Safynia and J. Raedler*, 2018.

23 P. Biesheuvel, B. Van Limpt and A. Van der Wal, *The journal of physical chemistry C*, 2009, **113**, 5636–5640.

24 P. M. Biesheuvel and A. van der Wal, *J. Membr. Sci.*, 2010, **346**, 256–262.

25 P. Biesheuvel, S. Porada, M. Levi and M. Z. Bazant, *Journal of solid state electrochemistry*, 2014, **18**, 1365–1376.

26 A. Hemmatifar, A. Ramachandran, K. Liu, D. I. Oyazun, M. Z. Bazant and J. Santiago, *arXiv*, 2018, **preprint**, xx.

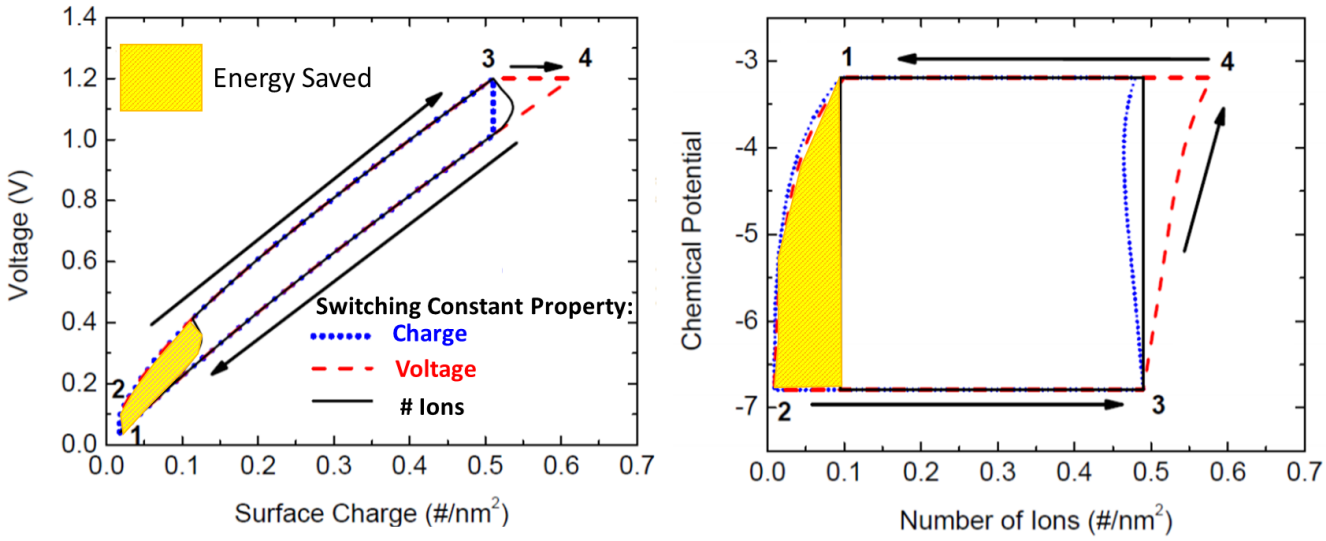

Graphical Abstract